https://doi.org/10.1038/s44454-025-00011-3

Modeling river and urban related microplastic pollution off the southern United States

Xing Zhou[1] ✉, Shuolin Xiao[2], Mireya Ramirez[1] & Annalisa Bracco[1,3]

The enclosed basin surrounding the Southern United States (the Gulf hereafter) faces increasing threats from microplastic (MP) pollution especially in its northern region. A Lagrangian particle-tracking model coupled with a high-resolution circulation model is used to investigate the short-term (30 days) transport of MPs in the northern Gulf over three years. The particle-tracking accounts for MP size and density and incorporates the influence of Stokes drift on floating MPs. Particle density is key in determining the distribution of settled MPs, with limited effects on non-settled MPs. The impact of Stokes drift on floating MP is negligible. River-sourced MPs emerge as dominant contributors to pollution. The simulated MP dispersal patterns are then linked to habitats and marine protected areas. A prominent accumulation zone is found west of the Mississippi River Delta, which overlaps with ecologically and economically important marine habitats, including Kemp's ridley sea turtles, red snapper and bottlenose dolphins.

Plastic pollution in the ocean is a growing environmental concern[1]. Plastic production has expanded over 260-fold since the mid-20th century[2,3], resulting in significant plastic accumulation in marine environments[4]. Rivers, streams, and runoff serve as terrestrial transport pathways, carrying pollutants, including plastics, from urban, agricultural, and industrial sources into the ocean. Most of these are microplastics (MPs), defined as plastic pieces ranging from 1 μm to 5 mm. MPs include synthetic polymers directly introduced into the environment as fine particles, though the majority arise from the degradation of larger plastics through physical abrasion, hydrolysis, photodegradation, and other processes[5,6].

MPs pose significant threats to aquatic ecosystems. Marine organisms can ingest MPs either selectively or accidentally, leading to accumulation through endocytosis or phagocytosis[7]. Ingested MPs then move through the food chain via trophic transfer[8]. Evidence of MP accumulation spans various taxa, from copepods[9,10] to top predators, including seals and whales[11,12]. The accumulation of MPs, coupled with their ability to adsorb harmful chemicals such as heavy metals[13,14], can lead to physiological impacts in marine organisms, including reduced growth, reproductive failure, and altered behavior[15,16].

Given these threats, effective management strategies of MP pollution are needed at both regional and global scales. Developing these strategies requires a deeper understanding of MP distributions. When observations are limited, advection-diffusion models, using Lagrangian or Eulerian frameworks, are commonly employed to simulate MP transport[17–19]. Model outputs, however, present several challenges. First, the diverse size, shape, and density of plastic particles result in distinct transport trajectories and fates. Many models either neglect or oversimplify these characteristics by categorizing particles as sinking, neutrally buoyant, or buoyant. Recent advances have introduced more systematic methods to consider particle diversity, including distribution-based approaches or explicit categorization of MPs based on their properties[20,21]. Second, MP sources and pathways are often underrepresented in simulations. While riverine inputs are typically included (e.g.,[22,23]), contributions from wastewater treatment plants (WWTPs) are rarely considered even though important MP point sources[24,25]. Additionally, non-point sources, such as atmospheric deposition[26] and stormwater runoff[27], are often excluded. Lastly, floating MPs can be influenced by Stokes drift. This is the case in the Arctic where Stokes drift facilitates movement from coastal waters to the open ocean[28,29]. In contrast, Stokes drift has been shown to have little effect on large-scale MP accumulation in subtropical regions[29].

In this work we focus on MP pollution in the northern Gulf of America, also known as Gulf of Mexico (the Gulf thereafter), due to its unique characteristics. As the terminus of the North America's largest river network, the Mississippi-Atchafalaya River System, the Gulf receives substantial MP input from upstream sources[30]. Additionally, the northern Gulf coastline is adjacent to large plastic manufacturing facilities, and urbanized regions that contribute significant MP loads[31]. Once MPs enter the coastal ocean, their fate is largely influenced by hydrodynamic processes, including

[1]School of Earth and Atmospheric Science, Georgia Institute of Technology, Atlanta, GA, USA. [2]Ralph S. O'Connor Sustainable Energy Institute, Johns Hopkins University, Baltimore, MD, USA. [3]CMCC Foundation, Euro-Mediterranean Center on Climate Change, Milan, Italy. ✉e-mail: xzhou473@gatech.edu

large freshwater plumes, currents driven by seasonally varying winds[32,33], and pervasive large mesoscale circulations such as the loop current (LC)[34,35]. The LC flows clockwise from the Caribbean through the Yucatán Channel, extending northward before exiting through the Florida Straits, and at irregular time intervals ranging from 2 to 20 months, it can detach large mesoscale anticyclones. The interaction between MPs and the dynamic circulation of the Gulf creates a complex transport environment, making it a representative region for studying land-to-ocean MP transport in areas influenced by strong river plumes and mesoscale circulation. Furthermore, the Gulf's economic importance, particularly its seafood and tourism industries, underscores the urgency of mitigating MP pollution in this region, as it threatens diverse species, ranging from endangered to commercially important[36,37]. Although plastic pollution in the Gulf has been recognized for decades, the region remains understudied in this context[38]. Observational efforts are largely confined to the nearshore environment, with field studies collecting samples on water, sediment, and biota along the coastline[37,39,40]. These observations reveal a widespread presence of MPs, predominantly in the form of fragments and fibers, in both water and sediment samples[38,41]. In contrast, data from offshore areas are extremely limited. One study has identified MPs in the ingestion of deep-pelagic crustaceans and fishes[42], and to date no studies have targeted MP concentrations in open-ocean water or sediment samples.Modeling efforts are also geographically limited. Existing studies have examined the transport of river-borne MPs originating from the Mississippi and Atchafalaya Rivers, as well as from other major waterways in Texas and Louisiana[23,43]. Their results consistently show strong southwestward transport of MPs along the Louisiana and Texas shelf, driven by regional currents and river plume dynamics. The knowledge gap regarding MP dispersal throughout the entire northern Gulf hinders the development of effective mitigation strategies and ecological protection policies. Modeling efforts can help in this regard, by providing guidelines as to where to expect large concentrations of MPs and by allowing to investigate which sources and processes are driving the modeled distributions.

Here, we build upon recent studies that have investigated coral and fish connectivity in the northern Gulf[44–46] and couple a Lagrangian particle-tracking model with a submesoscale-permitting (1 km horizontal resolution) regional ocean model to investigate the transport of MPs originating from major rivers and WWTPs associated with large urban areas in the northern Gulf. The model accounts for MP density and size variations influencing sinking and floating behavior, as well as the effects of Stokes drift. The spatial distribution and temporal variation of MPs in the northern Gulf is examined considering influences from river discharge, ocean currents, and the seasonal variability of the LC. Lastly, we link the simulated MP spatial distribution with marine protected areas (MPAs) and habitat data to assess the risks posed by MP pollution to different MPAs and various marine species.

Results

To analyze the MP distribution in the northern Gulf, after performing the model simulations described in the Methods Section, we divided the area into 10×10 km boxes and tallied settled and unsettled MPs separately within each box for all simulations conducted from 2014 to 2016. Accounting for the fact that each particle released from rivers represents 5×10^9 items and each particle released from WWTPs represents 7600 MP items, we then generated spatial concentration maps of MP for each case, which we discuss separately next.

Settled MPs

The concentration map of settled MPs is shown in Fig. 1. For this case, we focused our analysis on Exp 1 and Exp 2, as the Stokes drift had minimal influence on settled MPs (Figs. S1 and S2). For MPs originating from WWTPs, the settled MPs exhibit strong localized accumulation near their release sites (Fig. 1a1, a2). We identified three distinct accumulation areas: the western Texas shelf shoreline, the region east of the Mississippi Delta, and the western Florida shoreline. Each accumulation area corresponds to MPs sourced from major urban corridors, including Corpus Christi to Greater Houston, New Orleans to Mobile, and the Tampa Bay area. Furthermore, comparing Exp 1 and Exp 2, Exp 1 shows a more widespread distribution of MPs along the coastline, whereas in Exp 2, most MPs settle closer to their release points.

MPs originating from rivers exhibit substantially greater concentrations in the Gulf compared to those from WWTPs due to the high discharge from the Mississippi and Atchafalaya Rivers. Both experiments show that MPs accumulate in nearshore areas, with concentrations increasing progressively toward the coastline. Notably, the Mississippi River Delta forms a distinct hotspot of accumulation. Focusing on high-concentration regions ($> 10^8$ items/km^2), Exp 1 reveals a broader and more diffuse spatial distribution, with MPs spreading across the northern Gulf and forming an expansive band along the coastline. In contrast, Exp 2 produces a more fragmented and localized distribution, with MPs settling in highly concentrated patches near their release points, reaching extreme concentrations ($10^9 \sim 10^{10}$ items/km^2).

Figure 2 presents the percentage of MPs that settled within 30 days relative to the total released MPs, along with their corresponding settling times. These two metrics were evaluated for each simulation, with the x-axis representing the release date. In Exp 1, both the percentage of settled MPs and their settling times exhibit substantial variability, with settlement rates ranging from 5 to 70% and settling times varying between 5 and 20 days. This variability is largely driven by seasonal fluctuations in river discharge and the depth of the surface mixed layer in the nearshore region. Moreover, compared to MPs originating from WWTPs, MPs sourced from rivers display a stronger variation in settlement rates and longer settling times, as river plumes transport MPs over longer distances before they settle. In contrast,

Exp 2, which incorporates both sinking and buoyant velocities, displays less variability over time. The percentage of settled MPs remains consistently high, around 80–85%, This is consistent with the vertical distribution estimated in the "Method" section (Fig. 10), where ~80% of MPs have sinking velocities. Exp 2 also show that most particles settling within 2 days of release. Moreover, the differences in settling percentage and settling time between MPs from WWTPs and those from rivers are minimal in Exp 2. The significant difference between Exp 2 and Exp 1 indicates that

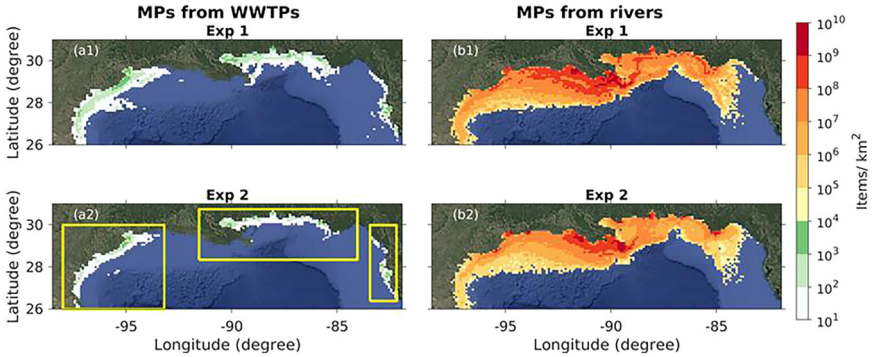

Fig. 1 | Spatial distribution of settled MPs in the northern Gulf for Exp 1 and Exp 2. The northern Gulf is divided into 10×10 km grid cells, with the settled MPs tallied within each cell for all simulations conducted from 2014 to 2016. a1–a2) Spatial distribution of settled MPs originating from wastewater treatment plants (WWTPs). b1–b2) Spatial distribution of settled MPs originating from rivers. The three yellow boxes in Fig. 1a2 indicate distinct accumulation areas for MPs sourced from WWTPs. From west to east, these areas are the western Texas shelf shoreline, the region east of the Mississippi Delta, and the western Florida shoreline.

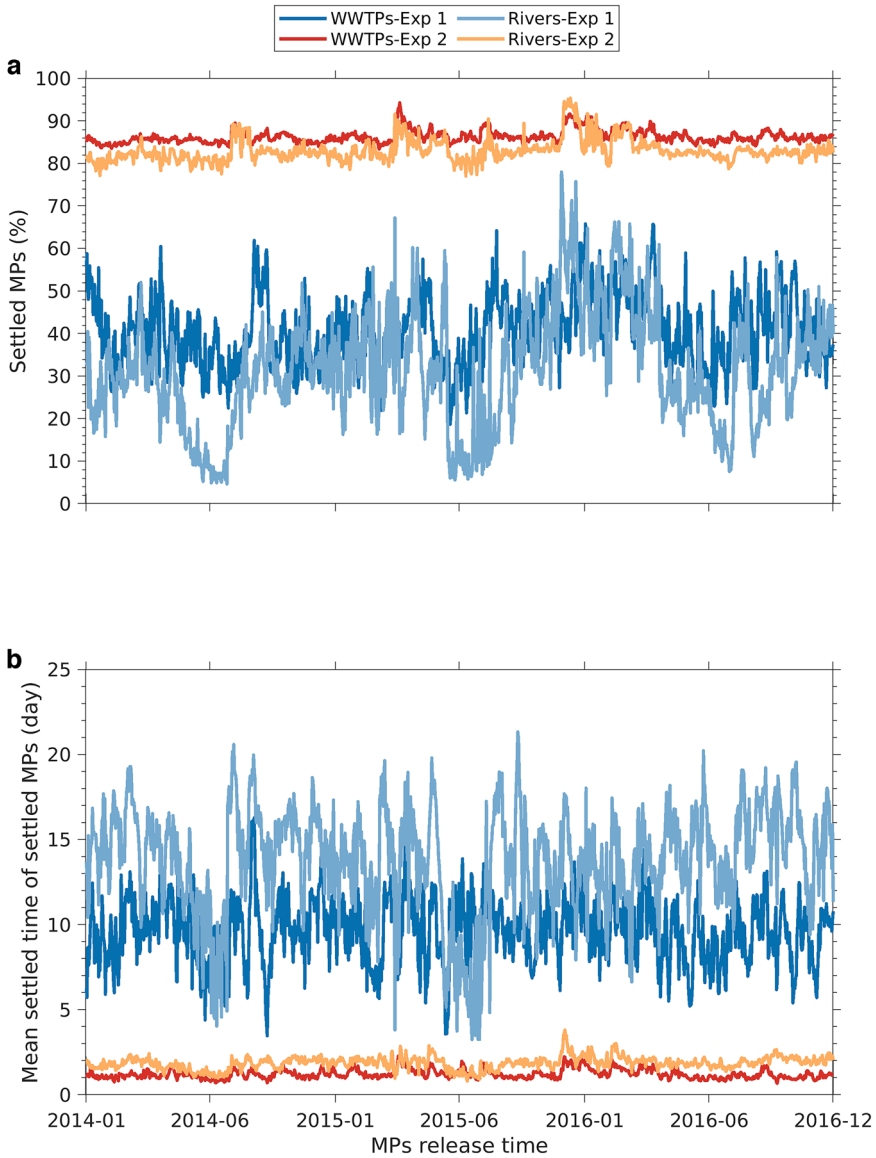

Fig. 2 | Time series of settling performance for MPs across all simulations. a Percentage of MPs that settled within 30 days, relative to the total number of MPs released. **b** Mean settling time of MPs that settled within 30 days. In both panels, the *x*-axis represents the release date of each simulation conducted from 2014 to 2016.

incorporating sinking velocities strongly influences the spatial and temporal patterns of settled MPs, with most particles rapidly settling to the bottom near the estuary within a short period.

Non-settled MPs

For MPs that remain suspended in the water column and do not settle during the 30-day tracking period, we generated, with the same approach used for settled MPs, vertically integrated concentration maps across all depths at the end of the simulation (Fig. 3). The spatial distribution of MPs originating from WWTPs closely resembles that of the settled MPs, indicating their localized accumulation characteristics. In contrast, MPs from rivers exhibit broad dispersal across the northern Gulf by the end of their 30-day tracking period. Concentrations of MPs decrease from north to east. The highest concentrations of MPs are simulated near the Mississippi River Delta and showing a clear westward propagation trend. Notably, Exp 1 shows higher MP concentrations throughout the northern Gulf compared to Exp 2 and Exp 3. This is consistent with Fig. 2, which shows that ~80% of released MPs settle in Exp 2 and Exp 3, whereas only about 30–40% settle in Exp 1, leaving a greater proportion of particles suspended in the water column.

The spatial distribution of non-settled MPs in the Gulf is closely linked to the region's circulation patterns. This includes the wind-driven shelf currents with superposed the variability associated to the LC and its detached eddies. Seasonal wind-driven circulation plays a crucial role in shaping the zonal MP accumulation patterns along coastal waters. For most of the year, winds predominantly blow from east to west, weakening notably during the summer months (June–July)[46]. Surface currents largely mirror this wind forcing, driving the westward transport of MPs. Consequently, a significant fraction of MPs from the Mississippi and Atchafalaya Rivers accumulates along the Texas shelf, forming a hotspot of plastic pollution. In contrast, MP transport east of the Mississippi Delta is minimal, with most eastward transport occurring during periods of weak winds and the influence of occasional clockwise mesoscale eddies. The LC and its detached eddies, on the other hand, can facilitate the transport of MPs from the coastal areas to the open Gulf, particularly east of the Mississippi Delta, where the LC's northward intrusion entrains MPs. In contrast, MPs west of the Mississippi Delta tend to remain in coastal waters.

Across all three experiments, the spatial distribution patterns of non-settled MPs appear broadly similar. The likeness between Exp 1 and Exp 2 likely stems from a similar vertical positioning, with most MPs remaining within the surface mixed layer for the entire 30-day tracking period. Figure 4 provides percentage density maps of MPs' vertical positions over this period, aggregated across all simulations. In both Exp 1 and Exp 2, most MPs accumulate above 15 m, with a more pronounced concentration near the

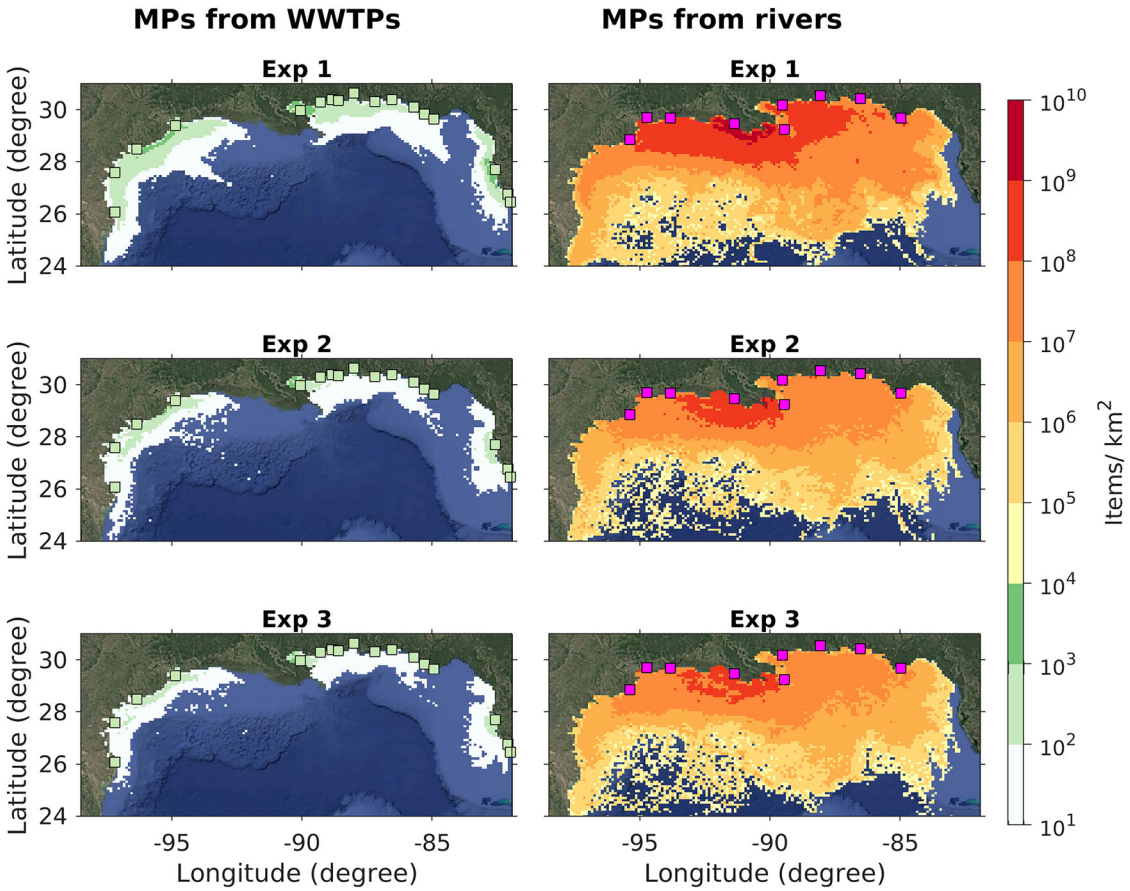

Fig. 3 | Spatial distribution of non-settled MPs at the end of their 30-day tracking period in the northern Gulf. From top to bottom, panels show results from Exp1, Exp2, and Exp3, respectively. In each row, the left panel displays MPs originating from WWTPs, and the right panel shows MPs originating from rivers.

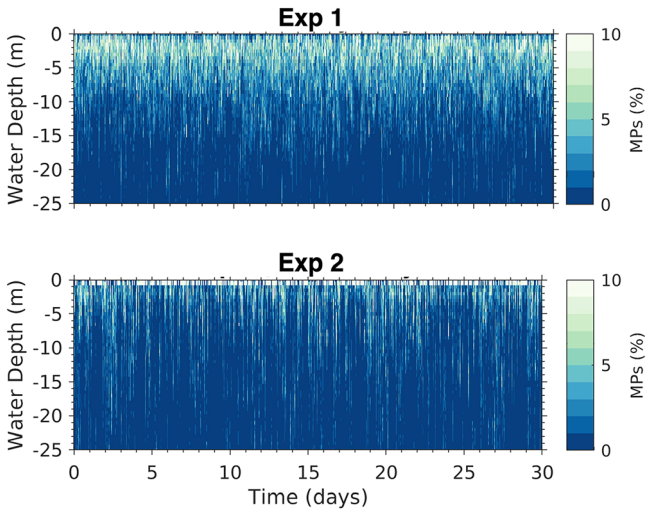

Fig. 4 | Vertical distribution of non-settled MPs over 30 days. Percentage density maps showing the vertical depth variation of non-settled MPs over their 30-day tracking period, aggregated across all simulations from 2014 to 2016.

surface in Exp 2 due to the buoyant characteristics of the MPs. In the northern Gulf, depths up to 15 m generally fall within the surface mixed layer, which extends to 60–90 m in winter and reduces to ~15–18 m in summer[47,48]. Consequently, most MPs in Exp 1 and Exp 2 experience similar physical conditions, resulting in analogous transport trajectories.

Therefore, assuming that MPs are neutrally buoyant is a reasonable approximation for both neutral and positively buoyant particles. Since MPs are released in very shallow waters, they are likely to remain within the surface mixed layer throughout the tracking period, unless significant internal or external mechanisms (e.g., strong sinking velocities or vertical transport associated with eddies) drive them out of it.

The similarity between Exp 2 and Exp 3 suggests that Stokes drift plays a relatively minor role. In the northern Gulf, wind speeds generally remain below 10 m/s, resulting in an estimated Stokes drift, based on Eq. 2 in "Method" section, of ~10^{-2} m/s. This estimate is consistent with results from global Stokes drift simulations[29] and regional studies in the Mediterranean Sea[49]. In comparison, surface currents in the northern Gulf have typical magnitudes of 10^{-1} m/s. Implementing the Stokes drift leads to a slight increase in the MP transport distance, a pattern also reported by Rühs et al.[49], but does not substantially affect where MP accumulates in the northern Gulf.

Seasonal variability

Figures 1 and 3 revealed a clear longitudinal structure in the spatial distribution of MPs. To further investigate the seasonal variability of these patterns, Hovmöller diagrams across three simulation years are shown in Fig. 5. They compare MPs originating from WWTPs and rivers and distinguish between settled and non-settled MPs. Settled MPs show relatively weak seasonal variability and strong spatial persistence. Consistent with the patterns shown in Fig. 1a1–a2, MPs from WWTPs accumulate in three distinct coastal zones in both Exp 1 and Exp 2. Exp 1 shows broader seasonal spread, especially along the western Texas shelf and the region east of the Mississippi Delta, while Exp 2 reveals more localized accumulation near the release sites, with minimal temporal variation (Fig. 5a1, a3). For MPs from rivers, Exp 1 displays moderate seasonal variability, with concentrations west of the Mississippi Delta fluctuating slightly by season (Fig. 5a2). In contrast, Exp 2 shows a highly localized and persistent signal near the

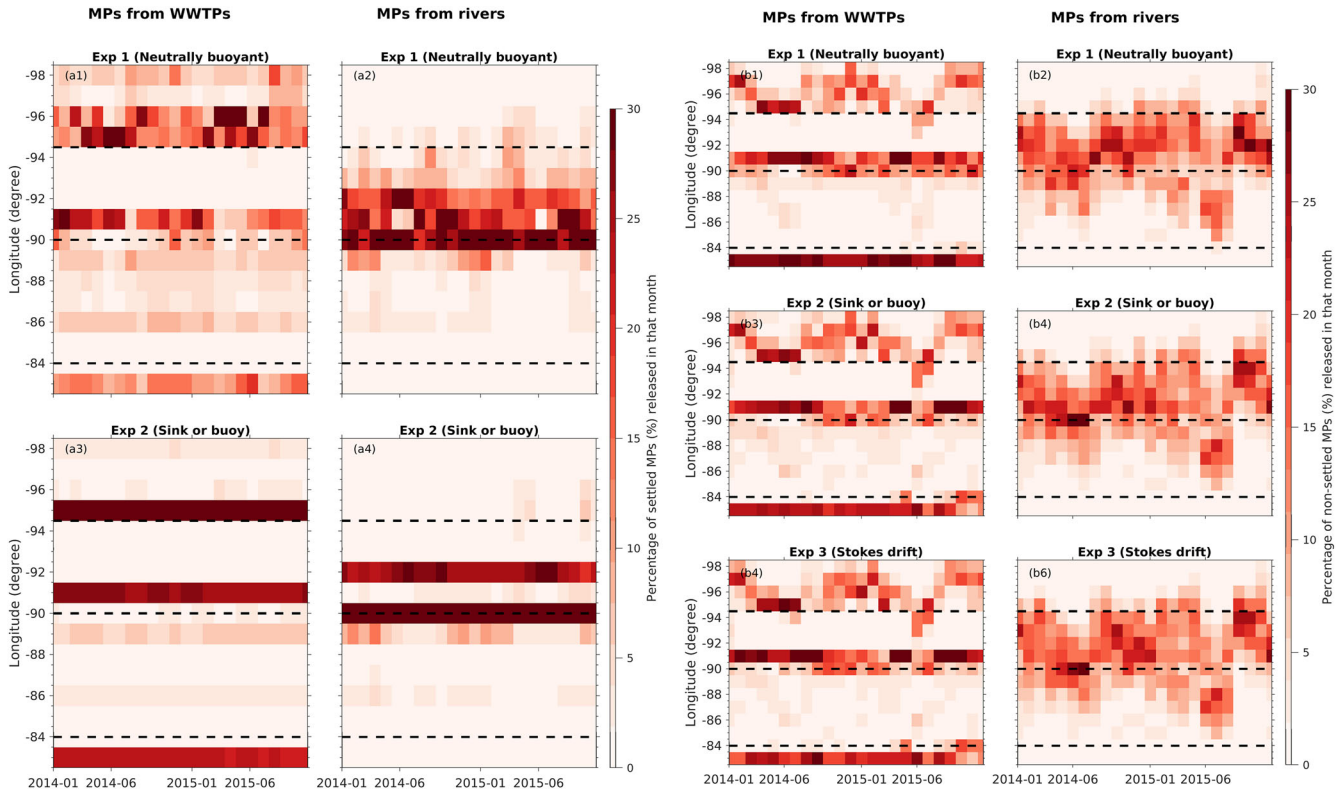

Fig. 5 | Seasonal and longitudinal variability in MP distributions (2014–2016) using Hovmöller diagrams. Each box displays the percentage of MPs within the corresponding longitude range, relative to the total number of settled or non-settled MPs released in that month. The left panel represents settled MPs, and the right panel shows non-settled MPs. The three black dotted lines from top to bottom mark the approximate longitudes of the Greater Houston, the Mississippi Delta, and the beginning of the western Florida shoreline, respectively.

Mississippi and Atchafalaya River mouths, with negligible seasonal changes (Fig. 5a4), suggesting that high sinking velocities dominate the spatial distribution of these settled MPs. In contrast, non-settled MPs show pronounced and consistent seasonal variability across all experiments, indicating the dominant influence of hydrodynamic forcing over particle characteristics (Fig. 5b). For MPs originating from WWTPs, dispersal patterns along the shoreline east of the Mississippi Delta and western Florida shift seasonally by ~1–2° in longitude. Along the western Texas shoreline, higher concentrations of MPs are observed near Houston during the summer months when longshore transport weakens. In other seasons, enhanced alongshore flow facilitates the transport of MPs originating from the Houston metropolitan area over longer distances along the coast (Fig. 5b1–b3).

For non-settled MPs from rivers, the model reveals a distinct west–east variation centered around the Mississippi Delta (Fig. 5b2–b4). MPs generally accumulate west of the Mississippi River Delta, between longitudes −90° and −94.5°, throughout most of the year. Exception to this behavior was found during the summers of 2014 and 2015, and the winter of 2016, when a greater portion of MPs were transported eastward. This seasonal variability of MPs is closely tied to the seasonal changes in wind-driven shelf currents.

Assessment of MPs exposure in MPAs and species habitats

Figure 6 illustrates the exposure of MPAs to MP pollution in the northern Gulf, considering both settled MPs and non-settled MPs. The spatial distribution maps show that most MPAs are in nearshore regions, where they are exposed to high concentrations of MPs from both WWTPs and rivers. Overall, the results indicate that most MPAs experience greater exposure to river-sourced MPs than to MPs from WWTPs.

Several MPAs warrant particular attention. The Texas Wildlife Refuge stands out with the highest MP stress index among all MPAs. While the land portion of this MPA is a designated wildlife refuge with minimal human activity, the marine portion is heavily exposed to MPs transported from the Mississippi and Atchafalaya Rivers. The West Florida Shoreline region is primarily impacted by MPs originating from WWTPs, suggesting that local pollution sources are dominant and that targeted management at the local level may be particularly effective. The Flower Garden Banks (FGB), the only offshore MPA in the northern Gulf, is also impacted by both floating and settled MPs. The average MP stress index at FGB is ~4.5 for settled MPs and increases to around 7 for non-settled MPs, with river-sourced MPs being the primary contributors. It is worth noting that FGB is located near the boundary between areas with and without MPs for the settled MPs map, which introduces some uncertainty in the modeled concentrations in this region.

In Fig. 7 we show the MP stress index calculated for the representative species in the Gulf (see "Methods" for its definition). Many species have a mixed life cycle (e.g., pelagic larvae and juveniles, and benthic adults) and therefore we report here the MP stress index for both settled and non-settled MPs originating from WWTPs and rivers. As to be expected, MPs from rivers dominate the exposure, with all species exhibiting MP stress index values >2 for non-settled MPs originating from rivers.

Among the species investigated, red snapper (RS) exhibits the highest MP stress, with values exceeding 6 for non-settled MPs and over 4 for settled MPs from river sources. Kemp's ridley sea turtle (KRST), a critically endangered species, shows similarly high MP stress from non-settled MPs, comparable to RS, while exposure to settled MPs is slightly lower (~2–3). Bottlenose dolphin (BD) and threadfin shad (TS), both fully pelagic species, also show notable stress levels, with MP stress indices for non-settled MPs around 4. Mexilhao Mussel (MM) exhibits a hybrid exposure pattern, with comparable MP stress from both river and WWTP sources.

To further evaluate the spatial relationship between MP pollution and species exposure, we mapped the overlap between

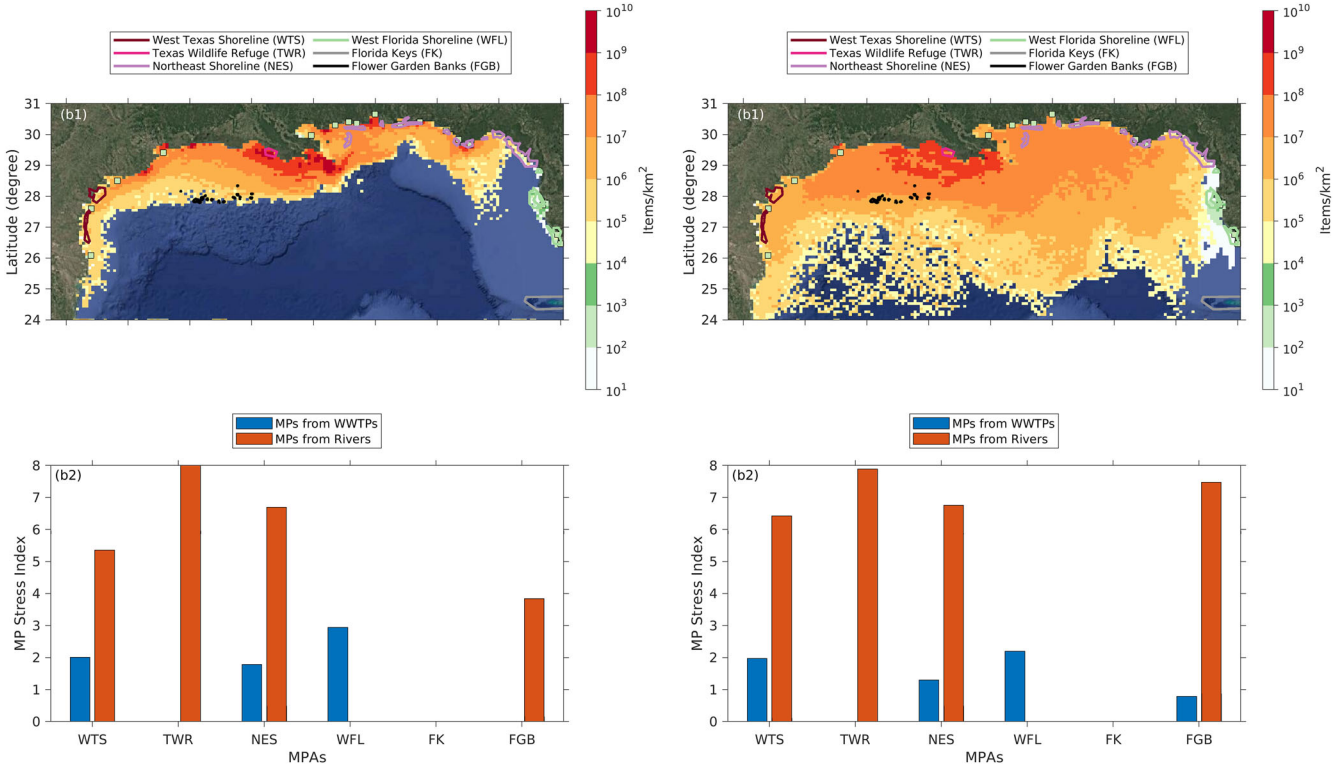

Fig. 6 | MPAs exposure to MPs pollution. Top panels: Locations of MPAs overlaid on the model-simulated spatial distribution of settled MPs (a1) and non-settled MPs (b1), respectively. Results are based on Exp 3, and the MP distributions represent the combined contributions from both WWTPs and river sources. MPAs are classified into six categories, shown in different colors, based on their geographic location and exposure to MP pollution. Bottom panels: Average MP stress index for MPAs in each category, corresponding to settled MPs (a2) and non-settled MPs (b2).

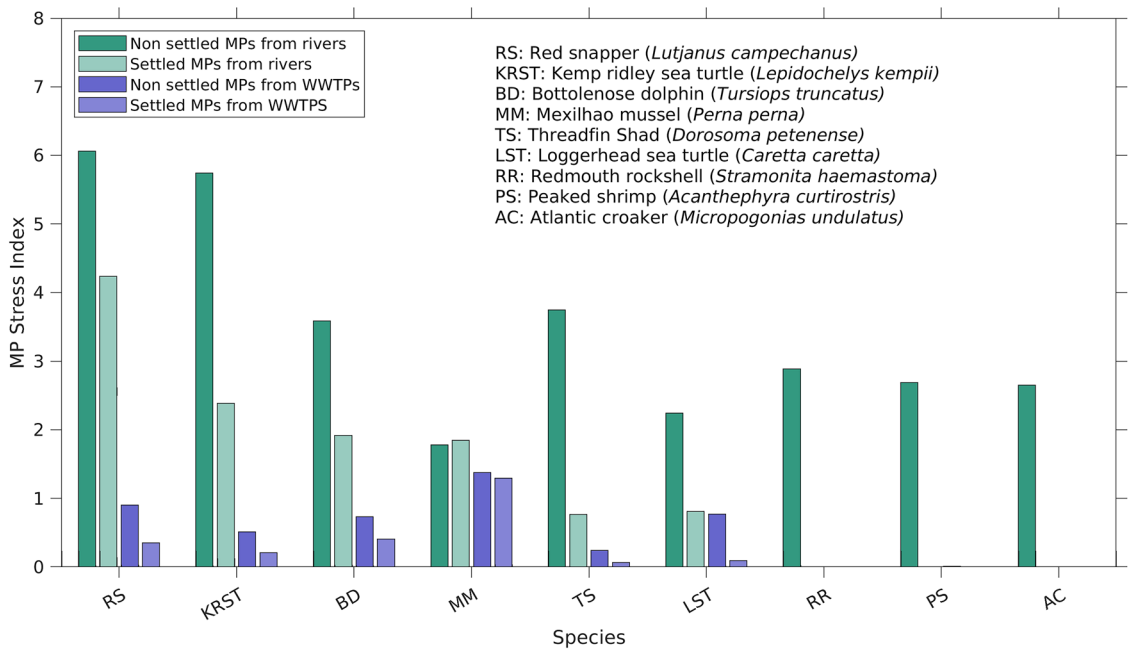

Fig. 7 | Spatial averaged MP stress index for different marine species. Among the species investigated, red snapper, Kemp's ridley sea turtle, bottlenose dolphin, and threadfin shad express high MP stress.

non-settled MPs originating from rivers and the habitats of three species with high MP stress indices (KRST, RS, BD) (Fig. 8). Most KRST habitats are primarily concentrated along the nearshore region west of the Mississippi River Delta and extend across the central Texas shelf. RS habitats exhibit a broader distribution, with approximately half located west of the Mississippi Delta, in a pattern like that of KRST, while the other half extends eastward into the nearshore waters of the northeastern Gulf. BD habitats are the most expansive, spanning both coastal and offshore areas across the northern Gulf on both the western and eastern sides.

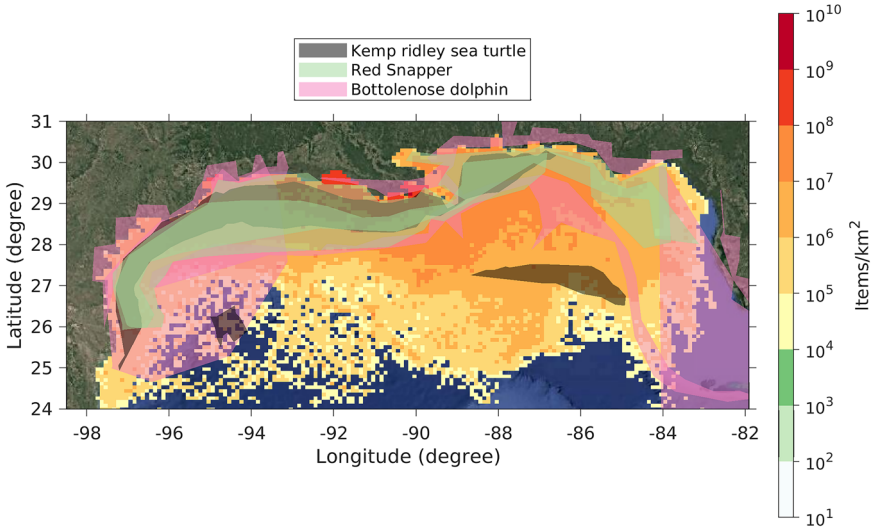

Fig. 8 | Spatial overlap between non-settled MPs and the habitats of highly impacted species. The distribution of non-settled MPs simulated in Exp3 from riverine sources is shown. Overlap is analyzed for three species: Kemp's ridley sea turtle, red snapper, and bottlenose dolphin.

The habitats of KRST and RS show substantial overlap with areas of high MP concentrations, particularly in the hotspot west of the Mississippi Delta, where concentrations exceed 10^8 items/km^2. This spatial alignment indicates the potential risk for exposure to MPs faced by these species. Although BD habitats also intersect regions with elevated MP concentrations, their distribution is more diffuse. All three species share habitats extending across the western Mississippi Delta and the Texas shelf, which likely contributes to the consistently high MP stress indices observed in Fig. 7.

Discussion

A first point of discussion is the confidence in our simulated MP concentrations and distributions. Our modeled distributions are informative because, on the one hand, this work responds to the recognized need for gaining a comprehensive understanding of MP distributions in the Gulf and for identifying areas at high ecological risk, as emphasized in recent literature[41], and, on the other, critical physical transport processes, such as river discharge and coastal and oceanic circulation, have been thoroughly validated in previous works[44–46].

Nonetheless, it is important to validate MP model outputs against field measurements, which is inherently challenging in the Gulf due to the scarcity and inconsistency of observational data. Almost all existing observations are limited to coastal regions, and Gulf-wide observational studies remain rare[38,41]. Moreover, there is no standardized methodology or consensus on reporting units for MP abundance, which makes it difficult to directly compare results across observational studies and between models and measurements.

Despite these limitations, we attempted to compare our modeled concentrations with the limited available field data, as well as with published estimates and modeling results from other studies. These comparisons support the model's ability to capture both the magnitude and spatial patterns of MPs. For example, Di Mauro et al.[39] reported concentrations of 4.8–18.4 items/m^3 off the Louisiana coast. Assuming a 15-m surface mixed layer, this corresponds to 7.2×10^7 to 2.7×10^8 items/km^2. Our predicted values in the same area are on the order of 10^8 items/km^2, showing consistency in magnitude. Wessel et al.[50] measured approximately 10^8 items/km^2 of MPs in Mobile Bay sediments, aligning with our modeled values for that region. In open ocean waters, Eriksen et al.[51] estimated surface MP concentrations of around 2.0×10^5 items/km^2. Our modeled values range from 10^4 to 10^6 items/km^2.

For spatial distribution, sand samples collected from loggerhead turtle nesting sites by Beckwith and Fuentes[37] and results from the NOAA NCEI Marine MP Product (Fig. S3, https://www.ncei.noaa.gov/products/microplastics accessed on Jun 2025) show a trend of higher MP accumulations in the area west of the Mississippi River Delta comparing to the east. This spatial pattern is also captured by our simulations and can be attributed to the longshore transport associated with freshwater plumes[23,43]. Finally, McEachern et al.[52] found that MP concentrations in sediments were higher than those in the water column in Tampa Bay. Our model captures this difference as well and shows that it likely extends across a broad region in the Gulf.

It is also important to notice the limitations and uncertainties of our study. One major limitation is the lack of comprehensive observational data on MP concentrations across the northern Gulf. While our model simulations were informed by measured MP concentrations from the Mississippi River and an overview of MP concentrations from 17 WWTPs across the United States[24], the absence of reliable regional measurements from rivers and WWTPs within the Gulf still hinders our ability to accurately quantify MP concentrations across grids and accumulation hotspots. This data gap is particularly critical for assessing exposure risks for marine organisms, as MP concentration levels are directly linked to ecotoxicological impact assessments.

Furthermore, our results reveal distinct transport and fate patterns that differ between negatively buoyant MPs and those with neutral or positive buoyancy. In this study, we adopted a generalized MP size and density distribution, adapted from Kooi and Koelmans[53], and found that most MPs exhibit strong negative buoyancy, leading to their rapid settlement in coastal areas. However, we acknowledge the sensitivity of MP density and size distributions. More comprehensive MP measurements in the Gulf would enable a better characterization of MP density and size distributions, improving our ability to quantify the percentage of MPs that settle and their residence time in the region.

Another model limitation involves the exclusion of key processes in the particle tracking model that may influence the fate of MPs. In our simulations, the buoyant velocity of MPs is calculated using the Stokes equation, and depends on particle size, density, and seawater properties. However, this approach does not account for several important processes that can alter MP density and size over time. One such process is secondary fragmentation, where exposure to ultraviolet radiation, mechanical stress, and microbial activity breaks down larger plastic particles into smaller ones. This transformation affects both their buoyancy and residence time in the water column[54,55]. Another critical process is biofouling, the colonization of MP surfaces by microorganisms. Over time, biofouling increases particle density, potentially converting initially buoyant MPs into neutrally buoyant or sinking particles, thereby altering their transport pathways[56–58]. Moreover, the simplified equation for estimating Stokes drift applied here may be suitable in open-ocean conditions, where waves are generally fully developed. However, this approach may introduce biases in coastal regions,

where environmental complexity arises from limited fetch, shallow water depth, and the influence of local currents shaped by coastal geomorphology. These factors can alter wave development and, consequently, the resulting Stokes drift. Previous studies have demonstrated that buoyant particles can be ejected from offshore accumulation zones and transported back toward the shoreline and beaches through the combined effects of wave-driven Stokes drift and windage[59–61]. In addition, observational and modeling studies have shown that the impact of Stokes drift on particle trajectories can be different than commonly parameterized at scale on the order of centimeters within the upper 10 m of the ocean[62,63]. To better capture the influence of Stokes drift on MP transport, particularly in nearshore areas in the Gulf, a fully coupled wave-ocean dynamic model would be required, along with higher-resolution to accurately represent shoreline morphology.

We have shown that MPs with neutral or positive buoyancy exhibit similar transport patterns over the simulation period of less than 30 days, suggesting that it is reasonable to assume neutral buoyancy when simulating the transport of both these kinds of MP. This assumption, however, may not be valid for long-term transport, as MP buoyancy may change over time, particularly in highly productive waters where biological processes can alter MPs' properties. Lastly, beaching of MPs also plays an important role, particularly along coastlines. Highly buoyant plastics may wash ashore, undergo photo-oxidative degradation and fragmentation, and then be re-entrained into the ocean by swash zone processes. These interactions are strongly influenced by coastal dynamics and morphodynamics. However, simulating nearshore currents and beach morphology remains a major challenge in coastal oceanography due to the complexity of these environments[64–66]. Coastal processes are shaped by multiple interacting factors, including breaking waves, rip currents, tides, wind, and buoyancy inputs. Moreover, accurately resolving plastic beaching and transport in these areas often requires extremely high spatial resolutions, ranging from centimeters to tens of meters, which is beyond the scope of most regional ocean models. Future research could incorporate these neglected processes to improve predictions of MP transport, ultimately providing a more comprehensive understanding of MP fate in dynamic coastal and ocean environments. Despite these limitations, our study provides a comprehensive analysis of MP transport in the northern Gulf. The novelty of our approach lies in the distribution-based method, which assigns density and size characteristics to individual particles. This allows for the simultaneous representation of diverse MP transport pathways and fate within a single simulation framework. In addition, we incorporate the effects of the Stokes drift and evaluate its relative contribution to MP transport. These methodological advancements improve our understanding of MP distributions and transports in the complex marine environment of the northern Gulf.

The simulated spatial distribution and seasonal variability of MPs in the northern Gulf offer valuable insights for informing management and conservation policies targeting MP pollution. The results highlight the Mississippi and Atchafalaya Rivers as the dominant sources of MPs, suggesting that mitigation efforts should prioritize controlling and potentially filtering riverine inputs. The spatial distributions of MPs also underscore the need for locally specific strategies. For example, MP pollution along the Florida coast is highly localized and effective strategies could be developed at the county level, while shallow and broad areas such as the Texas shelf would require cross-jurisdictional coordination and integrated management.

In terms of conservation policies and ecosystem impact, our work has highlighted that most MPAs undergoes localized threats with relation to MP pollution. In other words, treatment or filtering at nearby sources would readily improve the stress level on the ecosystem. However, long-distance river-borne MP transport can poses risks to offshore MPAs such as FGBs National Marine Sanctuary, but it is usually not considered and needs to be noted. Long-distance offshore MP transport is generally more variable and dependent on the LC system (LC and the detached eddies) conditions, and therefore more difficult to capture accurately even with targeted observational campaigns. Conservation measures should consider species-specific exposure and vulnerability, and in this regard RS (high economic value) and KRST (critically endangered status) should be regarded as top conservation priorities, being both subject to high MP exposure.

Methods

Ocean model

We employed the Coastal and Regional Ocean Community model (CROCO v1.3) to simulate the circulation features in the northern Gulf over a 3-year period. CROCO is a modeling platform built upon ROMS AGRIF[67]. It is designed for studying regional, coastal, and nearshore ocean dynamics across different time scales (events to multi-decadal periods) and spatial scales (kilometric to metric resolutions). The model domain covers the Gulf north of 24°N, extending from 98°W to 82°W, with 70 sigma layers for vertical resolution and 1 km horizontal resolution (Fig. 9a). Open boundary conditions were set at the southern and eastern boundaries, with nudging to the Hybrid Coordinate Ocean Model—Navy Coupled Ocean Data Assimilation (HYCOM-NCODA) Analysis system[68] every 3 h.

Following the approach in Sun et al.[69], we considered 10 rivers with the largest average discharge along the northern Gulf coastline of the United States (Fig. 9b). We imposed all river discharges as a southward volume flux from the north side of the model column grid near the river mouths. The river discharge data were obtained from the U.S. Geological Service (USGS) and the U.S. Army Corps of Engineers (USACE). The freshwater flux is distributed across the column of water of the closest grid point to the actual river mouth with largest flux at the surface and an exponential decay moving from the surface toward the ocean bottom. The southward momentum associated with the (3 h changing) fresh water flux is added to the meridional component of the velocity field at the different vertical levels. The meteorological forcing used to drive the ocean model was sourced from the Navy Global Environmental Model (NAVGEM), and is the same adopted by the HYCOM-NCODA analysis. Meteorological variables include 10-m wind, surface shortwave radiation, surface downward longwave radiation, precipitation, 2-m air temperature, and relative humidity. The model also included ten harmonic tidal constituents (M2, S2, N2, K2, K1, O1, P1, Q1, Mf, and Mm) from the TPXO-7 global tidal model. Initial conditions were extracted from an existing run with a similar configuration[69].

The CROCO simulation covered the years 2014–2016. The period was chosen because it includes times when circulation in the northern Gulf was strongly affected by Loop Current variability (summers of 2014 and 2015), as well as a period when the circulation was close to its climatological mean with limited interference from the Loop Current in the norther portion of the domain (2016). Additionally, it spans both strong and weak river discharge conditions, including flooding conditions following an El Nino winter (2016) (Fig. 9b).

The results of CROCO simulations in nearly identical configurations were validated against observational data for water temperature and salinity in the upper 300 m of the water column in Liu et al.[48] and for near-bottom velocity by Lopera et al.[46]. Additionally, modeled surface currents were compared to the HYCOM analysis (GOMI0.04/EXPT_31.0 and GOMI0.04/EXP_32.5 experiments) in Zhou et al.[45]. While CROCO, configured as a free-evolving model, does not exactly follow the observed flow evolution, it consistently represents well the mesoscale variability and the circulation in a statistical sense[48,69].

Particle tracking model

Ichthyop v3.3.16 (https://github.com/ichthyop/ichthyop, accessed August 10, 2024) was used as the particle tracking tool in this study. This offline Lagrangian particle tracking module is designed to simulate the movement of particles in three dimensions.

For this study, we adopted and modified the buoyancy functionalities of Ichthyop to use a Stokes equation (Eq. 1) to calculate the buoyant/upward or sinking/downward vertical velocity for MP particles according to:

$$W_b = g \times d \times d \times \frac{\rho_{water} - \rho_{MPs}}{18\mu} \quad (1)$$

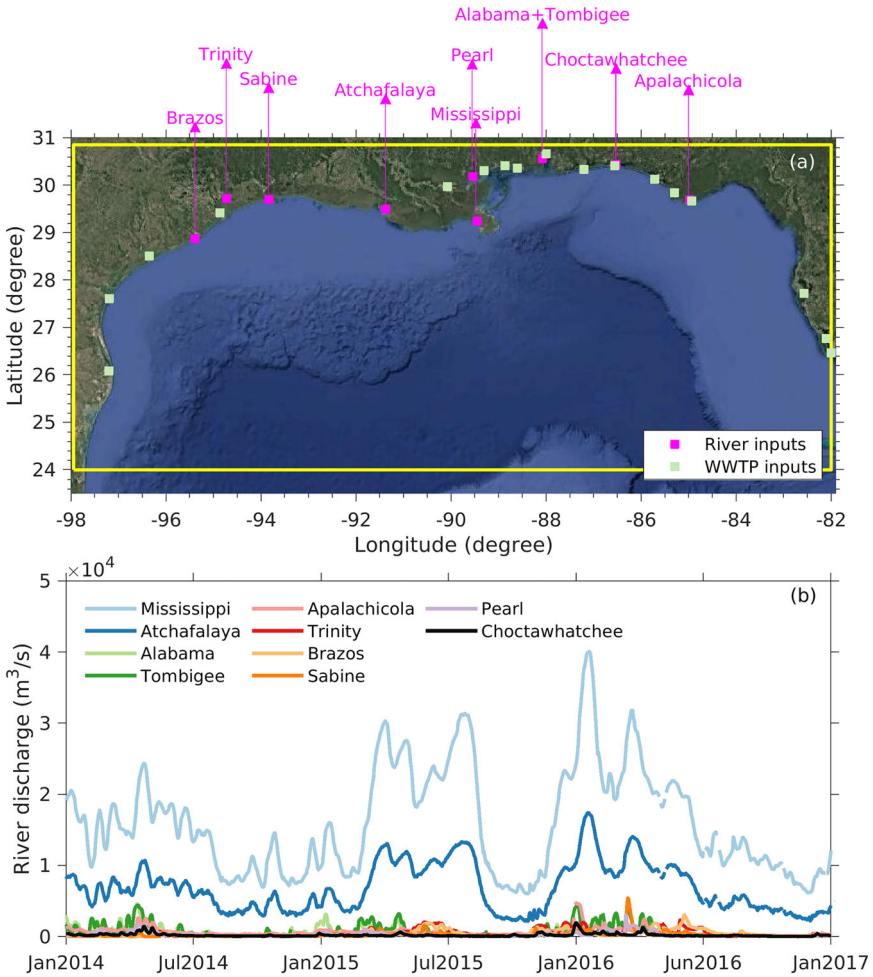

Fig. 9 | Model domain with terrestrial MP inputs and river discharge data. a The model domain of the northern Gulf is shown by the yellow box, with purple and light green boxes indicating the locations of river and WWTP inputs, respectively. **b** Daily river discharge data for the 10 rivers included in this study.

Where W_b is the buoyant or sinking velocity (m/s), g is the gravitational force (m/s^2), d is the size (equivalent diameter) of MPs (m), ρ_{water} and ρ_{MPs} are the density for the sea water and MPs (kg/m^3), and μ is the water molecular viscosity $(g \cdot m^{-1} \cdot s^{-1})$. Equation 1 was applied individually, with each particle assigned a density and size randomly sampled from the distribution adapted from Kooi and Koelmans[53] and described in the following section, reflecting the diversity of environmental MPs. By assigning each particle its own buoyant or sinking velocity, this approach is more comprehensive and realistic in representing different types of MPs (e.g., polyamide, polypropylene, polystyrene). Shape, on the other hand, was not individually considered as commonly done in studies at the scales considered here because different MP shapes require different functionalities to calculate buoyant or sinking velocity[53,70]. Also, MPs of shapes other than spherical typically exhibit much lower buoyant or sinking velocities due to their distinct geometric characteristics[71]. To include a range of buoyant and sinking velocities as wide as possible, our study specifically focuses on spherical MPs. All MP particles were approximated as spherical with a diameter d, which can be thought of as an equivalent diameter, considering shape factors.

In this study, we applied the "stick" option for particles that reach the coastline boundary to avoid uncertainties associated with the beaching of MPs. This means that particles reaching the boundary are fixed to it and excluded from further transport. Addressing beaching typically requires more refined coastal dynamics and morphodynamics, which are beyond the scope of this study.

Size and density distribution of MPs

The density and size distribution of MPs adopted are based on fitted data from Kooi and Koelmans (2019). Their analysis incorporated the densities of the most common MP polymer types (PA, PE, PET, PP, PS, PVA, PVC) observed in aquatic environments, thus reflecting realistic density variations. Regarding size distributions, Kooi and Koelmans[53] collected the published data from various locations, including water and sediment samples across different polymer types. To the authors' knowledge, their dataset represents the most comprehensive yet straightforward characterization available and has been widely adopted in addressing the complexity and diversity of MPs encountered in natural scenarios. Although extensively utilized, it should be noted that their density and size distributions rely on fitted mathematical functions, which may not perfectly represent conditions in our specific study area. Nonetheless, given existing data limitations, this approach provides the best available approximation.

Based on the given density and size distribution (Fig. S4), an estimated velocity distribution was derived using Eq. 1, assuming a standard seawater density of $1.025 kg/m^3$ (Fig. 10) The results indicate that ~80% of the MPs have a density higher than seawater. The sinking velocities of these particles are on the order of $10^{-2} m/s$ .For comparison, the absolute values of ocean vertical velocity range from $5 \times 10^{-4} m/s$ to $2 \times 10^{-3} m/s$[45], suggesting that gravitational settling may dominate over vertical oceanic currents for sinking particles. Buoyant velocities are typically of the order of $10^{-3} m/s$. Although this is lower than the sinking velocities, it is still sufficient for buoyant MPs to rise from a depth of 50 m to the surface in less than one day under quiescent conditions. These differences in sinking and buoyant velocities imply distinct transport pathways and spatial and temporal distribution patterns for settled and non-settled MPs, which was discussed in the "Results" section.

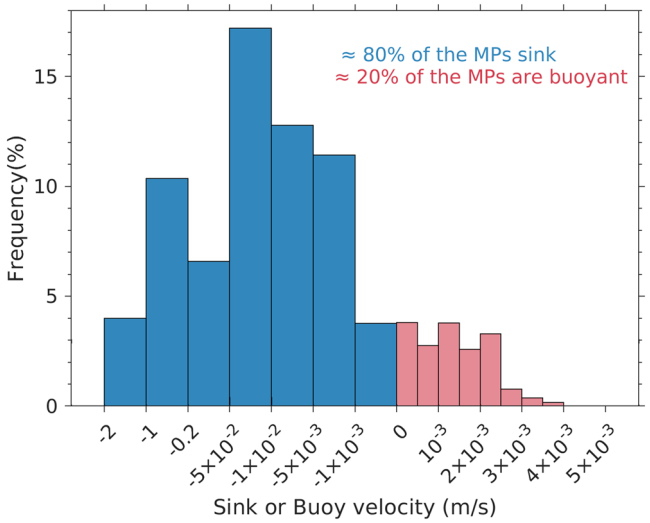

Fig. 10 | Estimated sinking and buoyant velocities of MPs in Exp 2. Frequency distribution of individual MPs sinking or buoyant velocities, calculated using Eq. 1 based on MP-specific density and size characteristics and assuming a standard seawater density of $1.025 kg/m^3$.

Table 1 | Description of particle tracking experiments

Experiments	Buoyant conditions	Stokes drift
Exp 1	Neutrally buoyant	Not considered
Exp 2	Sinking or buoyant velocity applied	Not considered
Exp 3	Sinking or buoyant velocity applied	Considered

Stokes drift

Some MPs, such as polyethylene and polypropylene, have densities lower than seawater, causing them to float to the ocean surface. As a result, these particles interact with the surface wave field, and the Stokes drift can alter their trajectory. For example, these floating MPs may move forward faster at the top of their orbits than backward at the bottom and spend more time in crests than in troughs due to the difference in velocity direction[72].

Here, we applied a "basic approximation" of the Stoke drift from Rühs et al.[49]. MP particles are advected by both the Eulerian current and a Stokes drift U_s parameterized as function of the wind speed at 10 m from the surface, U_{10}, according to:

$$U_s = 0.0014 \times F^{\frac{17}{150}} \times U_{10}^{\frac{58}{75}} \quad (2)$$

where F is the fetch, defined as the distance from a lee shore or the distance over which the wind blows with constant velocity. In this study, we used the minimum distance from the coastline as a proxy for F, simplifying our calculations without significantly affecting the computed Stokes drift. This approximation is justified by U_s being small compared to the Eulerian current in coastal areas and not sensitive to changes in F in the open sea, where the wave field is fully developed. Equation 2 is a simplified form derived from the JONSWAP spectrum[73,74] following Webb and Fox-Kemper et al.[75]. The Stokes drift was only considered for the first layer of the model.

Experiment design

Rivers and WWTPs are regarded as significant sources of MP inputs to the ocean[38,76]. Here, we released particles daily to represent a specified quantity of MPs at the mouths of river estuaries and WWTP locations. The density and size of particles released from both river and WWTP-based sources were randomly sampled from the same distribution described above, meaning that we assume no statistical differences in the properties of MPs originating from rivers and WWTPs. The number of particles released daily was calculated using the following equation:

$$P_i = D_i \times C_{MPs} \times \frac{1}{R_{P:MPs}} \quad (3)$$

Where P_i is the number of particles released daily from each river or WWTPs, D_i is the daily discharge from the river or WWTPs. C_{MPs} is the concentration of MPs in the river or WWTP effluent. $R_{P:MPs}$ is a proportionality factor that represents how many MP items each model particle represents. This factor is necessary because it is computationally infeasible to simulate every individual MP item entering the Gulf. Instead, we release a limited number of particles ($\sim 2 \times 10^4$ particles per day) to maintain computational efficiency while still capturing the key transport and dispersion patterns of MPs. $R_{P:MPs}$ is estimated by dividing the total observed MP loading into the Gulf by the number of model particles released. For example, if observational data suggest that 2×10^8 MP items enter the Gulf per day, then each model particle would represent 10,000 items (i.e., $R_{P:MPs} = 10,000$ items/particle), ensuring that we maintain around 2×10^4 particles in the simulation. We dynamically estimated this factor based on MP loading from both rivers and WWTPs, as further described next.

The river discharge was obtained from USGS and USACE. However, measurements of C_{MPs} in rivers, especially those with low discharge, are scarce. We adopted a simplified approach by applying an average concentration of 41.36 items/L, obtained from measures at seven sites along the Mississippi River, to all rivers used in this study[30].

The WWTP locations and discharges were identified using a map product of all U.S. available at https://www.waterandwastewater.com/us-wastewater-treatment-plants-map/ (accessed Dec 2024). Due to the complex geomorphology of the coastline and the model resolution, it was not feasible to release particles precisely at each WWTP location. Recognizing that MP inputs from WWTPs are closely related to human activities, we aggregated WWTPs into 18 individual groups based on urbanization belts along the Gulf and summed their discharge values. Particles were then released at these aggregated locations (Fig. 9a, Table S1). For concentration of MPs in WWTP effluents, we used 0.05 items/L based on data from Mason et al.[24], which overviewed MP concentrations from 17 WWTPs across the United States. It is important to note the significant uncertainty in C_{MPs} for WWTPs, as MP concentrations in U.S. WWTP effluents are relatively low compared to other countries (e.g., 4200–42,000 items/L in France[77] and 4000–9000 items/L in China[78]).

Although MP inputs from rivers and WWTPs are both recognized as major sources of ocean MPs, their daily loadings in the Gulf differ significantly in magnitude, primarily due to differences in discharge volumes (Fig. 9b and Table S1). Based on the above D_i and C_{MPs} values, rivers contribute MP loadings to the Gulf on the order of 10^{14} items/day, whereas WWTPs contribute only about 10^6 items/day. These estimates for rivers and WWTPs are consistent with findings reported in the literature (10^{12}–10^{14} items/day for the Mississippi River from Cizdziel[30]; and 2–4.4×10^6 items/day for WWTPs from Mason et al.[24]; Sun et al.[79]; and Ross et al.[76]). Despite the lower contributions of WWTPs compared to rivers, their absolute loading numbers are substantial and justify individual investigation of their transport and fate in the Gulf. To balance computational cost while ensuring a sufficient number of particles for effective tracking, we dynamically adjusted $R_{P:MPs}$ based on MP loadings from rivers and WWTPs. and set $R_{P:MPs} = 5 \times 10^9$ items/particle for rivers and 7600 items/particle for WWTPs, resulting in approximately 2×10^4 particles released daily from rivers and WWTPs, respectively.

We performed three experiments summarized in Table 1. By comparing Exp 1 and Exp 2 we can investigate the role of the sinking/buoyant velocity on the transport of MPs, as well as understand the differences in the fate of various environmental MPs in the northern Gulf. Exp 3 allows us to quantify the influence of Stokes drift on the transport of MPs, particularly for highly buoyant types.

Table 2 | MP stress index and corresponding MP concentration levels from Sun and Zhang[25]

MP level	Concentrations (item/km^2)
1	1–10
2	10–10^2
3	10^2–10^3
4	10^3–10^4
5	10^4–10^5
6	10^5–10^6
7	10^6–10^7
8	>10^7

In each release, particles were tracked for up to 30 days from their initial release. If, at any point during the 30-day tracking period, the vertical distance between the MPs and the ocean bottom was less than 0.5 m, the particle was considered settled at the bottom and immediately removed from the simulation. A 30-day tracking period was selected as a compromise for computational efficiency. While we acknowledge that MPs typically persist in the water for much longer[50,80], this approach, considered together with the daily release of particles, ensures a balance between computational feasibility and realism.

Assessment of MPs threat to marine habitats

The modeled MP results are integrated with marine habitat data for various species and NOAA's MPAs data in the Gulf to assess the risk posed by MP pollution to different pelagic marine species and MPAs. Selected species hold either ecological significance or economic and recreational value in this region, and all have been documented to be affected by MP pollution. They include the critically endangered KRST (*Lepidochelys kempii*) and the commercially important RS (*Lutjanus campechanus*). Table S2 lists the sources of the habitat areas for all selected species. Habitat areas were digitized and overlaid onto spatial distribution maps of MP concentration to identify species at risk of MP exposure. A similar process was applied to the MPAs dataset, which was retrieved from the NOAA database (https://marineprotectedareas.noaa.gov/dataanalysis/mpainventory/, accessed April 2025). The MPA regions were digitized from GIS geoplot files, and only MPAs of visible significance and without overlapping coordinate errors were retained for mapping. We then determine the stress level caused by MPs on habitats and MPA regions following the approach for categorizing MP stress introduced by Sun and Zhang[25]. Assessing the risk of MPs in the ocean is complicated by the lack of toxicological assessments of MPs in control (background) and current (real) concentrations. Indeed, the MP toxicity does not depend only on the MPs concentration, age, size, shape, composition, additives, etc., but also on the impacted organism characteristics (species, age, sex, reproductive stage, etc.). To complicate things further, MPs can have compounded toxicity with other pollutants.

One way forward, proposed by Sun and Zhang[25] and adopted in our work, is to determine the stress intensity due to MPs based on two factors: (1) the "30 × 30 Initiative" that calls for action to protect 30% of the ocean area by 2030; and (2) the MP concentrations in the global ocean. The higher the MP concentrations, the greater the stress, and in the absence of measurements of MP stress in actual ecosystems, a threshold for stress is set to be the concentration that would represent a 30% coverage.

In this framework, the modeled data for the global distribution of MP concentrations are ranked in a discontinuous manner (divided in levels 1–8, starting at 1 item/km^2, with each subsequent level increasing by an order of magnitude as in their Fig. 1 and Table 2 here), and no level or combination of levels provides an exact 30% coverage. Thus, levels 6–8 are selected as delimiting the area with high stress, which corresponds to a 13.45% of the global ocean, and largely covers known and highly publicized plastic debris zones. If the range was extended to level 5, the stress area would occupy 46.13% of the global ocean, which is too large of an area to be informative. Given that in the global dataset the majority of the Southern Ocean is characterized by MP concentrations in levels 1–3, and that the Southern Ocean has the lowest MP concentrations[81], these three levels identify low stress concentrations. The remaining levels are designated as medium stress.

High stress levels lead to increased health risks for marine organisms. These include physical disturbances such as entanglement caused by large-sized MPs[82], as well as complex biological and chemical interactions. For example, MPs that accumulate in sediments can alter sediment stability and disrupt benthic microbial communities[83]. Ingestion of MPs can lead to bioaccumulation and serious health effects, potentially resulting in death in large marine fauna[84]. Using this framework, we calculated the MP stress index for each habitat area and MPA to evaluate the potential threats posed by MP pollution.

Data availability

Meteorological forcing data used for the high-resolution regional ocean model can be obtained from https://data.hycom.org/datasets/force/NAVGEM/. River discharge data are available at: https://geo.gcoos.org/river_discharge/. Open boundary condition data can be accessed from https://www.hycom.org/data/gomu0pt04/expt-50pt1. The WWTP data used in the Lagrangian particle-tracking model are available at: https://www.waterandwastewater.com/us-wastewater-treatment-plants-map/. The extracted habitat and MPA data, along with the processed model output—including particle distribution data that can be converted to MP concentrations using a post-processing program—are available at https://zenodo.org/records/15685532. Raw model outputs, including hydrodynamic conditions from the regional ocean model and simulated MP distributions from the Lagrangian particle-tracking model, are available upon reasonable request. These datasets are extremely large due to high spatial resolution and temporal frequency.

Code availability

The official version of the Lagrangian particle-tracking model is available at https://ichthyop.org/. The specfic version used in this study, along with the pre- and post-processing codes, is available through Zenodo https://zenodo.org/records/15685532.

Received: 5 May 2025; Accepted: 5 July 2025;
Published online: 28 August 2025

References

1. Cole, M., Lindeque, P., Halsband, C. & Galloway, T. S. Microplastics as contaminants in the marine environment: a review. *Mar. Pollut. Bull.* **62**, 2588–2597 (2011).
2. Plastics Europe. Plastics — the facts 2022: an analysis of European plastics production, demand and waste data; (2022).
3. Chen, B. et al. Global distribution of marine microplastics and potential for biodegradation. *J. Hazard. Mater.* **451**, 131198 (2023).
4. Agbekpornu, P. & Kevudo, I. The risks of microplastic pollution in the aquatic ecosystem. In *Advances and Challenges in Microplastics* (IntechOpen, 2023).
5. Koelmans, A., Kooi, M., Law, K. L. & Van Sebille, E. All is not lost: deriving a top-down mass budget of plastic at sea. *Environ. Res. Lett.* **12**, 114028 (2017).
6. Al Harraq, A. & Bharti, B. Microplastics through the lens of colloid science. *ACS Environ. Au* **2**, 3–10 (2021).
7. Yan, N., Tang, B. Z. & Wang, W. X. Cell cycle control of nanoplastics internalization in phytoplankton. *ACS Nano* **15**, 12237–12248 (2021).
8. Wang, W. X. Environmental toxicology of marine microplastic pollution. *Camb. Prisms Plast.* **1**, e10 (2023).
9. Aytan, U., Esensoy, F. B. & Senturk, Y. Microplastic ingestion and egestion by copepods in the Black Sea. *Sci. Total Environ.* **806**, 150921 (2022).
10. Xu, J. et al. Unpalatable plastic: efficient taste discrimination of microplastics in planktonic copepods. *Environ. Sci. Technol.* **56**, 6455–6465 (2022).

11. Lusher, A. L. et al. Microplastic and macroplastic ingestion by a deep diving, oceanic cetacean: the True's beaked whale Mesoplodon mirus. *Environ. Pollut.* **199**, 185–191 (2015).
12. Nelms, S. E., Galloway, T. S., Godley, B. J., Jarvis, D. S. & Lindeque, P. K. Investigating microplastic trophic transfer in marine top predators. *Environ. Pollut.* **238**, 999–1007 (2018).
13. Tourinho, P. S., Kočí, V., Loureiro, S. & van Gestel, C. A. Partitioning of chemical contaminants to microplastics: Sorption mechanisms, environmental distribution and effects on toxicity and bioaccumulation. *Environ. Pollut.* **252**, 1246–1256 (2019).
14. Weng, N., Meng, J., Huo, S., Wu, F. & Wang, W. X. Hemocytes of bivalve mollusks as cellular models in toxicological studies of metals and metal-based nanomaterials. *Environ. Pollut.* **312**, 120082 (2022).
15. Ferreira, P., Fonte, E., Soares, M. E., Carvalho, F. & Guilhermino, L. Effects of multi-stressors on juveniles of the marine fish Pomatoschistus microps: gold nanoparticles, microplastics and temperature. *Aquat. Toxicol.* **170**, 89–103 (2016).
16. De Sá, L. C., Oliveira, M., Ribeiro, F., Rocha, T. L. & Futter, M. N. Studies of the effects of microplastics on aquatic organisms: what do we know and where should we focus our efforts in the future? *Sci. Total Environ.* **645**, 1029–1039 (2018).
17. Hardesty, B. D. et al. Using numerical model simulations to improve the understanding of micro-plastic distribution and pathways in the marine environment. *Front. Mar. Sci.* **4**, 30 (2017).
18. Cai, C., Zhu, L. & Hong, B. A review of methods for modeling microplastic transport in the marine environment. *Mar. Pollut. Bull.* **193**, 115136 (2023).
19. Moodley, T., Abunama, T., Kumari, S., Amoah, D. & Seyam, M. Applications of mathematical modelling for assessing microplastic transport and fate in water environments: a comparative review. *Environ. Monit. Assess.* **196**, 667 (2024).
20. Huang, Y. et al. Quantifying the influence of size, shape, and density of microplastics on their transport modes: a modeling approach. *Mar. Pollut. Bull.* **203**, 116461 (2024).
21. Shettigar, N. A., Bi, Q. & Toorman, E. Assimilating size diversity: population balance equations applied to the modeling of microplastic transport. *Environ. Sci. Technol.* **58**, 16112–16120 (2024).
22. Liu, R., Wang, T., Li, J., Liu, X. & Zhu, Q. Simulation of seasonal transport of microplastics and influencing factors in the China Seas based on the ROMS model. *Water Res.* **244**, 120493 (2023).
23. Summers, E., Du, J., Park, K. & Kaiser, K. Quantifying the connectivity of microplastic pollution in the Texas–Louisiana coastal area. *ACS ES&T Water* 4, 2482–2494 (2024).
24. Mason, S. A. et al. Microplastic pollution is widely detected in US municipal wastewater treatment plant effluent. *Environ. Pollut.* **218**, 1045–1054 (2016).
25. Sun, D. & Zhang, L. Where are the global ocean priority conservation areas under the most severe threat from microplastics? *Mar. Policy* **168**, 106326 (2024).
26. Xiao, S., Cui, Y., Brahney, J., Mahowald, N. M. & Li, Q. Long-distance atmospheric transport of microplastic fibres influenced by their shapes. *Nat. Geosci.* **16**, 863–870 (2023).
27. Sutton, R. et al. Understanding microplastic levels, pathways, and transport in the San Francisco Bay region. San Francisco Estuary Institute, SFEI Contribution No. 950 (2019). https://www.sfei.org/documents/understanding-microplastic-levels-pathways-and-transport-san-francisco-bay-region.
28. Isobe, A. et al. Selective transport of microplastics and mesoplastics by drifting in coastal waters. *Mar. Pollut. Bull.* **89**, 324–330 (2014).
29. Onink, V., Wichmann, D., Delandmeter, P. & van Sebille, E. The role of Ekman currents, geostrophy, and stokes drift in the accumulation of floating microplastic. *J. Geophys. Res. Oceans* **124**, 1474–1490 (2019).
30. Cizdziel, J. Microplastics in the Mississippi River and Mississippi Sound. Mississippi Water Resources Research Institute-Final Grant Report for award, (G16AP00065) (2020).
31. Tunnell, J. W., Dunning, K. H., Scheef, L. P. & Swanson, K. M. Measuring plastic pellet (nurdle) abundance on shorelines throughout the Gulf of Mexico using citizen scientists: establishing a platform for policy-relevant research. *Mar. Pollut. Bull.* **151**, 110794 (2020).
32. Schiller, R. V., Kourafalou, V. H., Hogan, P. & Walker, N. D. The dynamics of the Mississippi River plume: impact of topography, wind and offshore forcing on the fate of plume waters. *J. Geophys. Res. Oceans* **116**, C06029 (2011).
33. Liu, G., Bracco, A., Sun, D. Offshore freshwater pathways in the northern Gulf of Mexico: impacts of modeling choices. *Front. Mar. Sci.* **9**, 841900 (2022).
34. Androulidakis, Y. et al. Offshore spreading of Mississippi waters: pathways and vertical structure under eddy influence. *J. Geophys. Res. Oceans* **124**, 5952–5978 (2019).
35. Brokaw, R. J., Subrahmanyam, B. & Morey, S. L. Loop current and eddy-driven salinity variability in the Gulf of Mexico. *Geophys. Res. Lett.* **46**, 5978–5986 (2019).
36. Phillips, M. B. & Bonner, T. H. Occurrence and amount of microplastic ingested by fishes in watersheds of the Gulf of Mexico. *Mar. Pollut. Bull.* **100**, 264–269 (2015).
37. Beckwith, V. K. & Fuentes, M. M. Microplastic at nesting grounds used by the northern Gulf of Mexico loggerhead recovery unit. *Mar. Pollut. Bull.* **131**, 32–37 (2018).
38. Shruti, V. C., Pérez-Guevara, F. & Kutralam-Muniasamy, G. The current state of microplastic pollution in the world's largest gulf and its future directions. *Environ. Pollut.* **291**, 118142 (2021).
39. Di Mauro, R., Kupchik, M. J. & Benfield, M. C. Abundant plankton-sized microplastic particles in shelf waters of the northern Gulf of Mexico. *Environ. Pollut.* **230**, 798–809 (2017).
40. Peters, C. A., Thomas, P. A., Rieper, K. B. & Bratton, S. P. Foraging preferences influence microplastic ingestion by six marine fish species from the Texas Gulf Coast. *Mar. Pollut. Bull.* **124**, 82–88 (2017).
41. Grace, J. K., Duran, E., Ottinger, M. A., Woodrey, M. S. & Maness, T. J. Microplastics in the Gulf of Mexico: a bird's eye view. *Sustainability* **14**, 7849 (2022).
42. Bos, R. P., Zhao, S., Sutton, T. T. & Frank, T. M. Microplastic ingestion by deep-pelagic crustaceans and fishes. *Limnol. Oceanogr.* **68**, 1595–1610 (2023).
43. Liang, J. H. et al. Including the effects of subsurface currents on buoyant particles in Lagrangian particle tracking models: Model development and its application to the study of riverborne plastics over the Louisiana/Texas shelf. *Ocean Model.* **167**, 101879 (2021).
44. Liu, G., Bracco, A., Quattrini, A. M. & Herrera, S. Kilometer-scale larval dispersal processes predict metapopulation connectivity pathways for Paramuricea biscaya in the northern gulf of Mexico. *Front. Mar. Sci.* **8**, 790927 (2021).
45. Zhou, X., Lopera, L., Roa-Varón, A. & Bracco, A. Modeling the larval dispersal and connectivity of Red Snapper (Lutjanus campechanus) in the Northern Gulf of Mexico. *Prog. Oceanogr.* **224**, 103265 (2024).
46. Lopera, L., Bracco, A. & Herrera, S. Physical connectivity between mesophotic areas in the northern Gulf of Mexico. *J. Geophys. Res. Oceans* **130**, e2024JC021753 (2025).
47. Mendoza, V. M., Villanueva, E. E. & ADEM, J. On the annual cycle of the sea surface temperature and the mixed layer depth in the Gulf of México. *Atmósfera* **18**, 127–148 (2005).
48. Liu, G., Bracco, A. & Sitar, A. Submesoscale mixing across the mixed layer in the Gulf of Mexico. *Front. Mar. Sci.* **8**, 615066 (2021).
49. Rühs, S. et al. Non-negligible impact of Stokes drift and wave-driven Eulerian currents on simulated surface particle dispersal in the Mediterranean Sea. *Ocean Sci.* **21**, 217–240 (2025).
50. Wessel, C. C., Lockridge, G. R., Battiste, D. & Cebrian, J. Abundance and characteristics of microplastics in beach sediments: insights into microplastic accumulation in northern Gulf of Mexico estuaries. *Mar. Pollut. Bull.* **109**, 178–183 (2016).

51. Eriksen, M. et al. Plastic pollution in the world's oceans: more than 5 trillion plastic pieces weighing over 250,000 tons afloat at sea. *PloS ONE* **9**, e111913 (2014).
52. McEachern, K. et al. Microplastics in Tampa Bay, Florida: abundance and variability in estuarine waters and sediments. *Mar. Pollut. Bull.* **148**, 97–106 (2019).
53. Kooi, M. & Koelmans, A. A. Simplifying microplastic via continuous probability distributions for size, shape, and density. *Environ. Sci. Technol. Lett.* **6**, 551–557 (2019).
54. Andrady, A. L. & Koongolla, B. Degradation and fragmentation of microplastics. *Plastics and the Ocean: Origin Characterization, Fate, and Impacts* (ed. Andrady, A.L.) 227–268 (Wiley, 2022).
55. George, M., Nallet, F. & Fabre, P. A threshold model of plastic waste fragmentation: new insights into the distribution of microplastics in the ocean and its evolution over time. *Mar. Pollut. Bull.* **199**, 116012 (2024).
56. Kooi, M., Nes, E. H. V., Scheffer, M. & Koelmans, A. A. Ups and downs in the ocean: effects of biofouling on vertical transport of microplastics. *Environ. Sci. Technol.* **51**, 7963–7971 (2017).
57. Kaiser, D., Kowalski, N. & Waniek, J. J. Effects of biofouling on the sinking behavior of microplastics. *Environ. Res. Lett.* **12**, 124003 (2017).
58. Capuano, T. A. et al. Oceanic realistic application of a microplastic biofouling model to the river discharge case. *Environ. Pollut.* **359**, 124501 (2024).
59. Yoon, J. H., Kawano, S. & Igawa, S. Modeling of marine litter drift and beaching in the Japan Sea. *Mar. Pollut. Bull.* **60**, 448–463 (2010).
60. Ko, C. Y. et al. Monitoring multi-year macro ocean litter dynamics and backward-tracking simulation of litter origins on a remote island in the South China Sea. *Environ. Res. Lett.* **13**, 044021 (2018).
61. Morales-Caselles, C. et al. An inshore–offshore sorting system revealed from global classification of ocean litter. *Nat. Sustain.* **4**, 484–493 (2021).
62. Laxague, N. J. et al. Observations of near-surface current shear help describe oceanic oil and plastic transport. *Geophys. Res. Lett.* **45**, 245–249 (2018).
63. Lodise, J., Özgökmen, T., Griffa, A. & Berta, M. Vertical structure of ocean surface currents under high winds from massive arrays of drifters. *Ocean Sci.* **15**, 1627–1651 (2019).
64. De Vos, A. et al. The M/V X-press pearl nurdle spill: contamination of burnt plastic and unburnt nurdles along Sri Lanka's beaches. *ACS Environ. Au* **2**, 128–135 (2021).
65. Moulton, M. et al. Exchange of plankton, pollutants, and particles across the nearshore region. *Annu. Rev. Mar. Sci.* **15**, 167–202 (2023).
66. Sutherland, B. R., DiBenedetto, M., Kaminski, A. & Van Den Bremer, T. Fluid dynamics challenges in predicting plastic pollution transport in the ocean: a perspective. *Phys. Rev. Fluids* **8**, 070701 (2023).
67. Auclair, F. et al. Some recent developments around the CROCO initiative for complex regional to coastal modeling. In *Comod 2018 Workshop on Coastal Ocean Modelling* 1–47 (2018, February). https://hal.archives-ouvertes.fr/hal-01947670.
68. Cummings, J. A. & Smedstad, O. M. Variational data assimilation for the global ocean. In *Data Assimilation for Atmospheric Oceanic, and Hydrologic Applications (Vol. II)* 303–343 (Springer, 2013).
69. Sun, D., Bracco, A. & Liu, G. The role of freshwater forcing on surface predictability in the Gulf of Mexico. *J. Geophys. Res. Oceans* **127**, e2021JC018098 (2022).
70. Schernewski, G. et al. Transport and behavior of microplastics emissions from urban sources in the Baltic Sea. *Front. Environ. Sci.* **8**, 579361 (2020).
71. Khatmullina, L. & Isachenko, I. Settling velocity of microplastic particles of regular shapes. *Mar. Pollut. Bull.* **114**, 871–880 (2017).
72. Van Sebille, E. et al. The physical oceanography of the transport of floating marine debris. *Environ. Res. Lett.* **15**, 023003 (2020).
73. Hasselmann, K. et al. Measurements of wind-wave growth and swell decay during the Joint North Sea Wave Project (JONSWAP). *Ergaenzungsh. Dtsch. Hydrogr. Z. Reihe A* 8(12), 1–95 (1973).
74. Hasselmann, K., Sell, W., Ross, D. B. & Müller, P. A parametric wave prediction model. *J. Phys. Oceanogr.* **6**, 200–228 (1976).
75. Webb, A. & Fox-Kemper, B. Wave spectral moments and Stokes drift estimation. *Ocean Model.* **40**, 273–288 (2011).
76. Ross, M. S. et al. Estimated discharge of microplastics via urban stormwater during individual rain events. *Front. Environ. Sci.* **11**, 1090267 (2023).
77. Yang, J. et al. Microplastics in different water samples (seawater, freshwater, and wastewater): removal efficiency of membrane treatment processes. *Water Res.* **232**, 119673 (2023).
78. Xiao, S., Liang, Y., Zhu, X., Kyes, S. & Cai, X. Are vehicle tires major contributors to microplastic emissions into the China seas? A simple model perspective. *Sci. Total Environ.* **920**, 171003 (2024).
79. Sun, J., Dai, X., Wang, Q., Van Loosdrecht, M. C. & Ni, B. J. Microplastics in wastewater treatment plants: detection, occurrence and removal. *Water Res.* **152**, 21–37 (2019).
80. Abreu, A. & Pedrotti, M. L. Microplastics in the oceans: the solutions lie on land. Field Actions Science Reports. The journal of field actions Special Issue, **19**, 62–67 (2019).
81. Suaria, G. et al. Floating macro-and microplastics around the Southern Ocean: results from the Antarctic Circumnavigation Expedition. *Environ. Int.* **136**, 105494 (2020).
82. Amelia, T. S. M. et al. Marine microplastics as vectors of major ocean pollutants and its hazards to the marine ecosystem and humans. *Prog. Earth Planet. Sci.* **8**, 1–26 (2021).
83. Marcharla, E. et al. Microplastics in marine ecosystems: a comprehensive review of biological and ecological implications and its mitigation approach using nanotechnology for the sustainable environment. *Environ. Res.* **256**, 119181 (2024).
84. Li, C., Zhu, L., Li, W. T. & Li, D. Microplastics in the seagrass ecosystems: a critical review. *Sci. Total Environ.* **902**, 166152 (2023).

Acknowledgements

This work was supported by the NOAA's National Centers for Coastal Ocean Science, Competitive Research Program and Office of Ocean Exploration and Research through award NA18NOS4780166 titled Connectivity of Coral Ecosystems in the Northwestern Gulf of Mexico (CYCLE). M.R. was supported by the President's Undergraduate Research Award from Georgia Institute of Technology.

Author contributions

X.Z., S.X., and A.B. conceived the study. X.Z. conducted all model simulations and performed the analyses with help from S.X. M.R. collected the data on MPAs and species-specific habitats. X.Z., S.X., and A.B. contributed to writing, reviewing, and interpreting the manuscript. All authors have read and approved the final manuscript for submission.

Competing interests

The authors declare no competing interests.

Additional information

Supplementary information The online version contains supplementary material available at https://doi.org/10.1038/s44454-025-00011-3.

Correspondence and requests for materials should be addressed to Xing Zhou.